JCB Journal of Cell Biology

REPORT

Neuralized-like protein 4 (NEURL4) mediates ADP-ribosylation of mitochondrial proteins

Maria Dafne Cardamone[1], Yuan Gao[1], Julian Kwan[1,2], Vanessa Hayashi[1], Megan Sheeran[1], Junxiang Xu[1], Justin English[1], Joseph Orofino[1], Andrew Emili[1,2], and Valentina Perissi[1]

ADP-ribosylation is a reversible post-translational modification where an ADP-ribose moiety is covalently attached to target proteins by ADP-ribosyltransferases (ARTs). Although best known for its nuclear roles, ADP-ribosylation is increasingly recognized as a key regulatory strategy across cellular compartments. ADP-ribosylation of mitochondrial proteins has been widely reported, but the exact nature of mitochondrial ART enzymes is debated. We have identified neuralized-like protein 4 (NEURL4) as a mitochondrial ART enzyme and show that most ART activity associated with mitochondria is lost in the absence of NEURL4. The NEURL4-dependent ADP-ribosylome in mitochondrial extracts from HeLa cells includes numerous mitochondrial proteins previously shown to be ADP-ribosylated. In particular, we show that NEURL4 is required for the regulation of mtDNA integrity via poly-ADP-ribosylation of mtLIG3, the rate-limiting enzyme for base excision repair (BER). Collectively, our studies reveal that NEURL4 acts as the main mitochondrial ART enzyme under physiological conditions and provide novel insights in the regulation of mitochondria homeostasis through ADP-ribosylation.

Introduction

Protein ADP-ribosylation is a widespread post-translational modification catalyzed by a family of enzymes known as ADP-ribosyltransferases (ARTs). ARTs covalently link ADP-ribose moieties, either as mono-ADP-ribose (MARylation or MAR) or poly-ADP-ribose chains (PARylation or PAR), on target proteins using NAD^+ as cofactor (Aravind et al., 2015; Cohen and Chang, 2018; Kraus, 2015). ADP-ribosylation can occur on several residues, including serine, glutamate, aspartate, arginine, lysine, and cysteine (Altmeyer et al., 2009; Barkauskaite et al., 2015; Bonfiglio et al., 2017; Leslie Pedrioli et al., 2018; McDonald and Moss, 1994; Messner and Hottiger, 2011; Van Ness et al., 1980; Palazzo et al., 2018; Vyas et al., 2014; Welsh et al., 1994). Depending on their conserved structural features, ARTs are classified as cholera toxin–like (ARTC) and diphtheria toxin–like (ARTD). The eukaryotic ARTDs, known as poly-(ADP-ribose) polymerases (PARPs) form the largest and most characterized group of ARTs, with 17 members and PARP1 (ARTD1) as founding member (Amé et al., 2004; Hottiger et al., 2010). Although the ARTD catalytic domain is structurally conserved, the protein sequence varies depending on the specific enzymatic quality of each member (Aravind et al., 2015; Cohen and Chang, 2018; Hassler and Ladurner, 2012; Otto et al., 2005). The full H-Y-E motif in the active center is present only in ARTDs capable of catalyzing PARylation (H/Y residues are required for binding to NAD^+, E for elongation), whereas enzymes performing MARylation contain a modified H-Y-I motif. Catalytically inactive enzymes lack the H (Aravind et al., 2015; Cohen and Chang, 2018; Hottiger et al., 2010).

In mammals, ADP-ribosylation is best known for its role in mediating the nuclear DNA damage response (Azarm and Smith, 2020; Gupte et al., 2017; Ray Chaudhuri and Nussenzweig, 2017). However, in the past two decades, a growing literature has indicated that ADP-ribosylation of proteins across all cellular compartments is relevant to a range of biological functions, including metabolism, inflammation, cancer, and aging (Bai and Cantó, 2012; Fehr et al., 2020; Kraus, 2015; Leung, 2014; Slade, 2020; Szántó and Bai, 2020; Vyas et al., 2013). While ARTs in the nucleus and cytoplasm have been extensively documented, the presence of ADP-ribosylation enzyme/s in the mitochondria remain controversial (Masmoudi and Mandel, 1989; Brunyanszki et al., 2016; Kadam et al., 2020). Although ART activity in mitochondria extracts from different tissues has been reported for decades (Burzio et al., 1981; Kun et al., 1975; Masmoudi and Mandel, 1987; Masmoudi et al., 1988; Richter et al., 1983), and despite widespread reports of ADP-ribosylated mitochondrial proteins (Herrero-Yraola et al., 2001; Hendriks et al., 2019; Martello et al., 2016; Pankotai et al., 2009; Vivelo et al., 2017; Williams et al., 2018), the specific

[1]Department of Biochemistry, Boston University School of Medicine, Boston, MA; [2]Center for Network Systems Biology, Boston University, Boston, MA.

Correspondence to Maria Dafne Cardamone: dafne.cardamone@hotmail.com; Valentina Perissi: vperissi@bu.edu.

nature of a mitochondrial ART has remained elusive. Among others, PARP1 has been investigated as a mediator of ADP-ribosylation in mitochondria based on its ability to interact with mitofilin (Rossi et al., 2009; Szczesny et al., 2014; Kadam et al., 2020). Based on PARP1's best known role as a regulator of the genomic DNA damage repair pathway in the nucleus, it was proposed that intramitochondrial PARP1 regulates mitochondrial DNA (mtDNA) stability by interacting with DNA ligase III (LIG3) on mtDNA (Brunyanszki et al., 2016; Rossi et al., 2009). However, there is no direct evidence that PARP1 enzymatic activity is required for the regulation of mtDNA maintenance or that PARP1 can mediate the PARylation of proteins involved in the DNA damage response or that of other targets identified as part of the mitochondrial PARylome. Moreover, PARP1 inhibition by olaparib in nonstressed HeLa cells eliminated nuclear PARylation without affecting extra-nuclear ADP-ribosylation signal (Nowak et al., 2020). This indicates that, even though PARP1 is activated under physiological conditions, its activity only accounts for nuclear modifications, thus raising the question of whether another ARTD family member or a previously unknown ART enzyme is responsible for mitochondrial PARylation.

In silico analyses aimed at identifying novel NAD⁺-using enzymes predicted the presence of an ART domain in the C-terminal domain of neuralized-like protein 4 (NEURL4; de Souza and Aravind, 2012). NEURL4 is currently classified as a member of the neuralized family based on the presence of six neuralized homology repeat (NHR) domains. The NHR domain is highly conserved from flies to mammals, and it is important in the mediation of protein–protein interactions. Four neuralized family members have been identified in mammals to date. NEURL1, NEURL2, and NEURL3 contain either a RING or a SOCS domain in addition to the NHR domains, and therefore serve as E3 ubiquitin ligases in a variety of physiological processes (Liu and Boulianne, 2017). NEURL4 and its fly homologue, *d*NEURL4, have not been associated with intrinsic ubiquitination activity, even though NEURL4 promotes ubiquitin signaling through interaction with the HECT E3 ubiquitin ligase HERC2 (Al-Hakim et al., 2012; Jones and Macdonald, 2015; Li et al., 2012; Loukil et al., 2017). Together, NEURL4 and HERC2 localize to the centrosome and interact with CP110 to regulate centrosome morphology and centriolar homeostasis via CP110 ubiquitin-dependent degradation (Al-Hakim et al., 2012). NEURL4/HERC2 complexes also regulate MDM2-p53 dimerization in response to DNA damage and Notch signaling via Delta-like 1 (Dll1)/Delta (Dl) recycling, even though in both cases HERC2 enzymatic activity appeared dispensable, and there is no evidence that NEURL4 regulates ubiquitination activity through PARylation as reported for other ART enzymes (Cubillos-Rojas et al., 2017; DaRosa et al., 2015; Imai et al., 2015; Yang et al., 2017).

Here we confirm the predicted enzymatic activity and report evidence that NEURL4 serves as a mitochondrial ART. We also discuss how the characterization of NEURL4's role in mediating the PARylation of many mitochondrial proteins has led to novel insights into the relevance of ADP-ribosylation for the maintenance of mitochondrial homeostasis.

Results and discussion

NEURL4 is a mitochondria protein with a functional ART domain

Comparative structure and genomic analysis aimed at uncovering novel NAD⁺-using enzymes have predicted the existence of a putative H-Y-E[D-Q] ART domain, similar to that of PARP1, within the C-terminal domain of NEURL4 (de Souza and Aravind, 2012; Fig. 1 A). Based on this prediction and previous reports of NEURL4 association with centromeres-associated factors (Al-Hakim et al., 2012; Loukil et al., 2017), it was suggested that NEURL4 might be regulating centrosomal assembly through PARP-like activity (Aravind et al., 2015; de Souza and Aravind, 2012). However, profiling of NEURL4 subcellular localization by immunohistochemistry in HeLa cells revealed it is predominantly found in mitochondria, as shown by colocalization with the mitochondria protein ATP5B (Fig. 1 B). In particular, the pattern of digestion by proteinase K, as compared with that of known markers of different mitochondrial compartments, indicated that NEURL4 localized to the mitochondrial matrix (Fig. 1 C). This was confirmed by immunogold labeling of NEURL4 showing its proximity to the cristae (Fig. 1 D). Based on the identification of a putative mitochondrial targeting sequencing within aa 1–65 of NEURL4 (see Fig. 1 A; Mitoprot software [Claros, 1995]), we predicted that mitochondrial import of NEURL4 would occur through the classic import pathway with cleavage of the N-terminal presequence. Processing was confirmed in transiently transfected HeLa cells by the accumulation of uncleaved NEURL4, as visualized by Western blot (WB) for the N-terminal Flag tag, upon transient knock-down of mitochondrial processing peptidases (MPPs) α and β by siRNAs (Fig. 1 E).

These results indicate that NEURL4 is a previously unrecognized mitochondrial protein and thus a promising candidate for mediating ADP-ribosylation in mitochondria. To confirm the predicted enzymatic activity, we performed in vitro PARylation assays with NEURL4 protein isolated from HeLa extracts, including PARP1 as positive control. As shown in Fig. 1 F, immunopurified NEURL4 mediated the synthesis of PAR chains in vitro, with its activity being potentiated in presence of activated DNA (Fig. 1 F, lane 1). A truncated form of NEURL4, lacking the predicted enzymatic domain at the C terminus, failed to generate PAR chains under the same conditions (Fig. 1 G), whereas the NEURL4 C terminus alone was sufficient to record ADP-ribosylation activity in vitro (Fig. 1 H).

NEURL4 enzymatic activity is required for mitochondrial PARylation

To further investigate the relevance of NEURL4 enzymatic activity and characterize its role in the mitochondria, we used CRISPR/Cas9 genome editing in Hela cells to generate two independent NEURL4 knock-out (N4-KO1 and N4-KO2) cell lines (Fig. 2, A and B). In both models, we observed a dramatic reduction of mitochondria-associated ADP-ribosylation in absence of NEURL4, as monitored by WB of mitochondrial extracts with anti-PAR antibody (Fig. 2 C). Because the mitochondrial pool of NAD⁺ is a shared cofactor of ART/Sirtuins enzymes, we reasoned that, if NEURL4 was a major user of NAD⁺ for ADP-ribosylation, the increased availability of mitochondrial NAD⁺

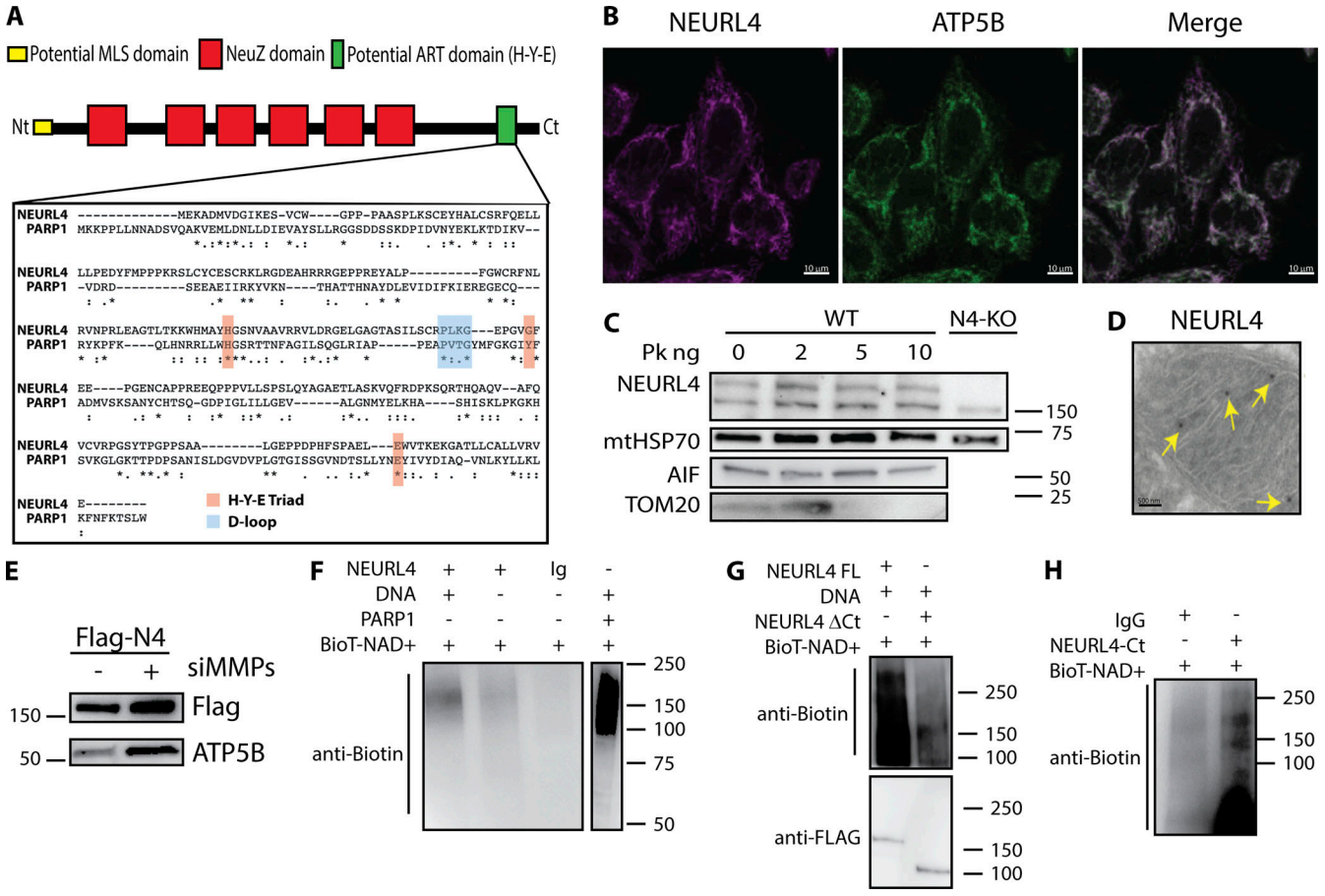

Figure 1. **NEURL4 is a mitochondrial protein with a functional ART domain. (A)** Graphical representation of NEURL4 known and predicted structural domains and alignment of the putative NEURL4 catalytic domain with the PARP1 catalytic domain showing conservation in the H-Y-E triad and D-loop. **(B)** NEURL4 localization to the mitochondria by IHF staining in HeLa cells as shown by costaining with the mitochondrial marker ATP5B. **(C)** Proteinase K protection assay showing NEURL4 localization to the mitochondrial matrix. Degradation patterns of TOM20, AIF1, and mtHSP70 are representative of proteins in the OMM, IMM, and matrix, respectively. **(D)** Mitochondria labeling by Immunogold EM for NEURL4 in HeLa cells. **(E)** Increased FLAG-NEURL4 stability upon down-regulation of MMPs (both MMPα and MMPβ) by specific siRNA. **(F–H)** In vitro PARylation assays showing NEURL4 ability to produce poly-ADP-ribosylation chains (F) via its Ct domain (G and H). Immuno-purified endogenous NEURL4, FLAG-NEURL4-ΔCt, or FLAG-NEURL4-Ct was incubated with biotin-NAD^+ in the presence or the absence of activated DNA. ADP-ribosylation was detected by WB anti-biotin. Loading controls for IP proteins were run on a different gel and tested with anti–FLAG-HRP antibody. Recombinant PARP1/ARTD1 was used as the positive control. The PARP1 reaction was run on the same gel and is shown here at lower exposure (F). MLS, mitochondria localization signal; Nt, N terminus; Pk, Proteinase K; ng, nanograms; siMMP, siRNA against MMPs (defined in E); FL, full length; OMM, outer mitochondrial membrane; IMM, inner mitochondrial membrane.

in the absence of NEURL4 could favor the activity of other enzymes such as NAD-dependent deacetylases. Indeed, we found that the acetylation level of mitochondrial proteins was significantly decreased in N4-KO cells, as expected in the presence of elevated mitochondrial sirtuins activity, whereas there was no difference in the abundance of nuclear acetylation (Fig. S1). Moreover, the dramatic decrease in mitochondria PARylation observed in N4-KO cells was rescued by reintroducing either the full-length NEURL4 or the putative catalytic domain alone (Fig. 2 D). These results confirmed that the NEURL4 C terminus domain is required for mediating mitochondrial PARylation. On the contrary, mitochondrial ADP-ribosylation did not require the activation of PARP1. As shown in Fig. 2 E, lane 4, mitochondria PARylation was not impaired by treatment with the specific PARP1 inhibitor olaparib (Menear et al., 2008). If anything, olaparib appeared to potentiate NEURL4-dependent mitochondrial PARylation, thus excluding the possibility of PARP1 being required for NEURL4-mediated activity. This experiment also revealed that mitochondrial ADP-ribosylation is sensitive to treatment with BGP-15, a nicotinic amidoxime derivate compound previously shown to accumulate in the mitochondria, reduce reactive oxygen species production, and function as a generic PARP inhibitor (Racz et al., 2002; Sumegi et al., 2017). Interestingly, ADP-ribosylation is not fully impaired by BGP-15, but the accumulation of high molecular weight PARylated proteins is greatly diminished, which suggests that elongation may be targeted (Fig. 2 E, lane 5). Together these data indicate that NEURL4 C terminus (Ct) domain is required for mediating mitochondria PARylation independently from PARP1. To further confirm that this is achieved through NEURL4 own enzymatic activity, we expressed the putative catalytic domain in *Escherichia coli* and performed in vitro PARylation assays. As shown in Fig. 2 F, the C terminus domain of NEURL4 mediates ADP-ribosylation in vitro, with its activity being abrogated by

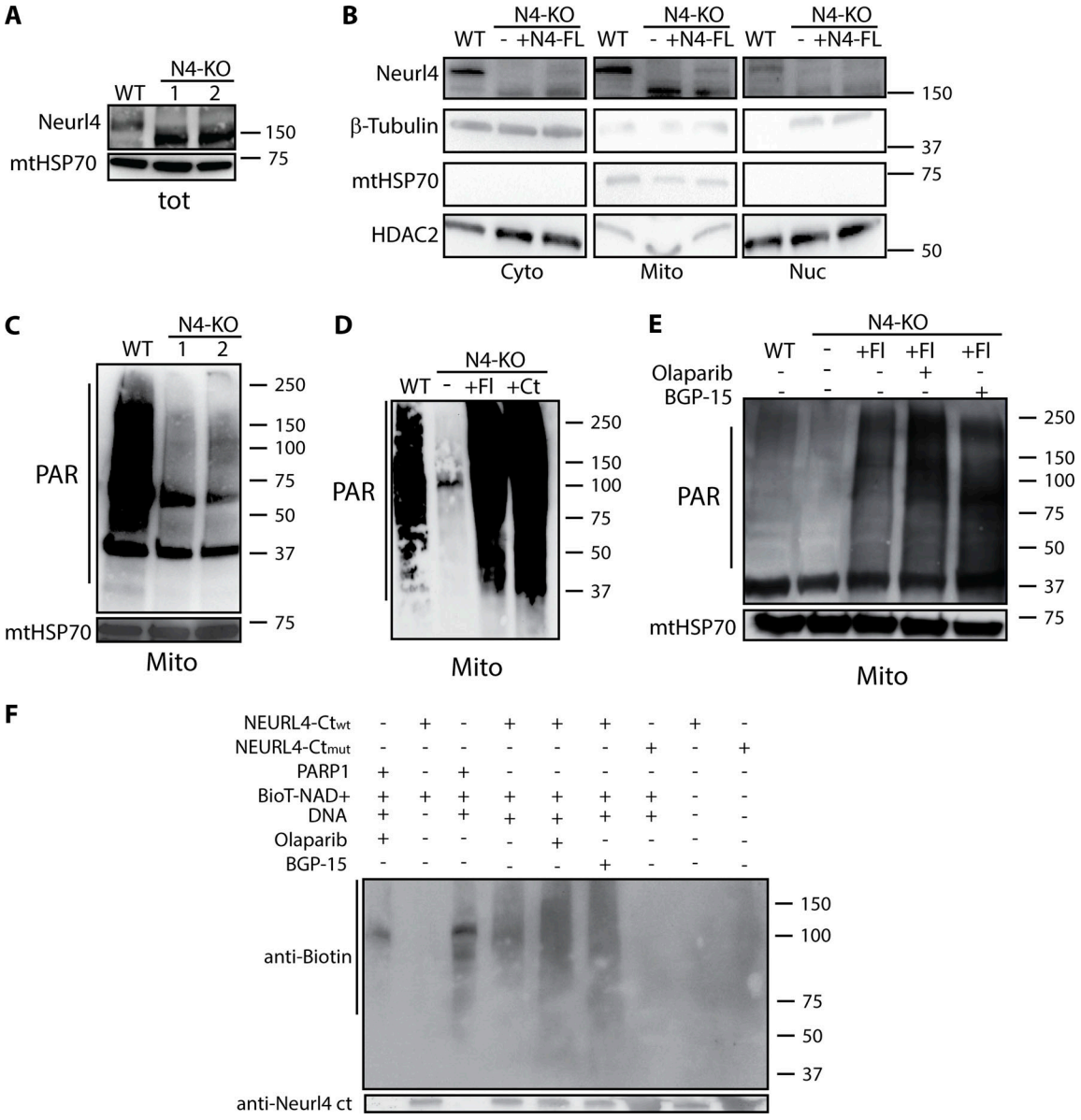

Figure 2. **NEURL4 enzymatic activity is essential for mitochondrial PARylation. (A and B)** Validation of NEURL4 KO cell lines generated by CRISPR/Cas9 genome editing of HeLa cells using two independent gRNA. WB of whole cell extracts (A) or fractionated cytosolic (Cyto), mitochondrial (Mito), and nuclear (Nuc) extracts (B). Rescue is performed by transient transfection with 200 ng full-length NEURL4 expressing vector. Efficiency of sub-cellular fractionation is confirmed by WB for β-tubulin, mtHSP70, and HDAC2. **(C)** WB anti-PAR on mitochondrial protein extracts showing that most mitochondrial PAR production is lost in untreated HeLa cells upon NEURL4 deletion. **(D)** WB anti-PAR on mitochondrial protein extracts from HeLa cells showing that loss of ADP-ribosylation in the absence of NEURL4 can be rescued reintroducing either full-length NEURL4 or the Ct domain alone (by transient transfection with 2 µg each). **(E)** NEURL4 enzymatic activity is inhibited by the generic PARP inhibitor BGP-15 (10 µg/ml) but not by PARP1/ARTD1 inhibitor olaparib (1 µM). **(F)** In vitro PARylation assays showing NEURL4 Ct domain ability to produce poly-ADP-ribosylation chains (wells 4, 5, and 6) compared with the catalytic mutant (well 7). FL, full length; tot, total extracts.

mutagenesis of key residues in the catalytic domain (HGS to AGA and ELEW to ALAA; see Fig. 1 A for sequence alignment). In this assay, the enzymatic activity of NEURL4 was not inhibited by olaparib, or by BGP-15. This further confirms that NEURL4 activity is distinct from that of PARP1 but leaves open the question of whether BGP-15–mediated inhibition of mitochondria ADP-ribosylation occurs through direct or indirect regulation of NEURL4 activity, which may occur through interactions outside of the catalytic domain or via modulation of reactive oxygen species production. Moreover, this assay confirmed that NEURL4 is activated by DNA (Fig. 2 F, lane 4). This suggested the possibility that NEURL4 could bind to DNA and play a role in mtDNA maintenance similar to that of PARP1 with nuclear DNA (Azarm and Smith, 2020).

NEURL4 is required for proper mtDNA maintenance

To investigate this hypothesis, we first confirmed by chromatin immunoprecipitation (ChIP) that NEURL4 binds to mtDNA

(Fig. 3 A). Then, we assessed the amount of poly-ADP-ribosylation associated with mtDNA in the presence or absence of NEURL4, and observed a significant decrease in N4-KO cells in comparison to their parental line (Fig. 3 B). Together, these results indicate that enzymatically active NEURL4 is present at the mtDNA. Because we did not observed a significant difference in mtDNA copy number when comparing N4-KO cells with their parental line (Fig. 3 C), it is unlikely that the loss of NEURL4 has any significant effect on DNA replication. Instead, amplification of the mtDNA by long-range PCR, using divergent primers, revealed a strong decrease in full-length, long amplicons, which is indicative of an increase in the frequency of mtDNA deletions in N4-KO cells as compared with WT (Fig. 3 D).

Compared with the nucleus, mitochondria DNA damage repair response relies mainly on DNA base excision repair/single-strand breaks repair (activity to contrast oxidative damage (van Houten et al., 2016; Prakash and Doublié, 2015). PARylation of the step limiting enzyme for mt-base excision repair resolution, the mitochondrial form of LIG3 (mtLIG3), was proposed as a regulatory strategy for mtDNA damage repair (Rossi et al., 2009). Thus, we asked whether mtLIG3 was a target of NEURL4. PARylation mtLIG3, as assessed by immunoprecipitation (IP)/WB, was found to be drastically reduced in both NEURL4-deficient cell lines (Fig. 3 E) and upon treatment with BGP-15, but not with olaparib (Fig. 3 F, lanes 2 and 3), confirming that NEURL4 is in fact required for the PARylation of mtLIG3. Moreover, in the absence of NEURL4, we observed increased accumulation of cytosolic mtDNA (Fig. 3 G) and corresponding activation of IL-1β processing and caspase activation (Fig. 3 H), as expected in the case of progressive accumulation of mutations and deletions ultimately leading to organelle dysfunction and mtDNA release in the cytosol, where it is recognized as a danger-associated molecular pattern by innate immune signaling pathways (Grazioli and Pugin, 2018).

Intriguingly, large-scale mtDNA deletions are widely regarded as a genetic biomarker for susceptibility to male infertility (Jiang et al., 2017; Karimian and Babaei, 2020; Kumar and Sangeetha, 2009). As this provided a possible mechanism for the difficulties we had encountered in the process of generating a whole-body NEURL4-KO mouse, we hypothesized that NEURL4-dependent regulation of mtDNA integrity is essential for maintaining male fertility. In support of this hypothesis, we observed that mtDNA derived from the sperm of NEURL4 male heterozygous mice showed an abnormally high rate of deletions (Fig. 3 I). NEURL4 heterozygous mice also presented reduced sperm count (Fig. 3 J) and increased sperm agglutination (Video 1 and Video 2), two gold standard markers of male infertility. Collectively, these results indicate that NEURL4 is required for mtDNA integrity both in vitro and in vivo and suggest this may be at least partially mediated by ADP-ribosylation of DNA damage repair factors like mtLIG3, similar to PARP1 function in the nucleus.

NEURL4-mediated mitochondria ADP-ribosylation is critical to maintain cellular homeostasis

Since mitochondria-associated PARylation is almost completely lost in N4-KO cells (see Fig. 2 C), we considered that NEURL4 may be broadly required for mediating the PARylation of a variety of mitochondrial proteins. To characterize the role of NEURL4 enzymatic activity in the regulation of mitochondrial functions, beyond the modulation of mtLIG3, we profiled the poly-ADP-ribosylation status of mitochondrial proteins in NEURL4 WT and KO cells via mass spectrometry–based quantitative proteomics using stable isotope labeling (SILAC). Putative targets were first enriched via binding to the WWE PAR-binding domain of Rnf146 (DaRosa et al., 2015) and then identified by liquid chromatography with tandem mass spectrometry (MS/MS). With this approach, we identified ∼170 putative targets defined as proteins with decreased poly-ADP-ribosylation in both KO cell lines and confirmed in two separate experiments (Fig. S2 A and Table S1). In agreement with the intra-mitochondrial localization, NEURL4 putative targets are enriched for proteins located in the matrix/inner mitochondrial membrane (Fig. 4 A). Moreover, overlay of our results with a previously reported total PARylome dataset (Martello et al., 2016) indicates that several of the mitochondrial proteins identified as ADP-ribosylated are putative NEURL4 targets (Table S1). Remarkably, among these targets are factors involved in the regulation of major mitochondrial functions (Fig. 4 B), including not only DNA damage repair but also carbon, fatty acid, and aa metabolism. As a representative factor, we confirmed that the ADP-ribosylation of the limiting enzyme in the urea cycle, CPS1, previously reported to be PARylated, is strongly reduced in N4-KO cells (Fig. S2 B). As expected in the presence of putative alterations in the functions of multiple factors/enzymes across diverse mitochondrial pathways, NEURL4-deleted cells present striking morphological and metabolic changes when compared with the parental line. Mitochondria in N4-KO cells are fragmented and present a donut-like shape that has been associated with loss of $\Delta\psi m$ in uncoupled mitochondria (Ding et al., 2012; Liu and Hajnóczky, 2011; Fig. 4 C). In accord with these phenotypic changes, assessment of mitochondrial bioenergetics by Seahorse respirometry showed a significant reduction in carbonyl cyanide-*p*-trifluoromethoxyphenylhydrazone (FCCP)–induced oxygen consumption rate (OCR), with both basal and maximal respiration being severely impaired in N4-KO cells (Fig. 4 D). Moreover, transcriptomic profiling of N4-KO cells by RNA sequencing (RNA-seq) revealed significant reprogramming of gene expression, with activation of gene programs important for metabolic adaptation to mitochondrial dysfunction (Fig. 4 E, Fig. S1 C, and Table S2). Overall, phenotypic and genomic characterization of NEURL4-deficient cells confirm NEURL4 relevance as a major mitochondrial enzyme and indicate that ADP-ribosylation of mitochondrial proteins by NEURL4 is critical for maintaining mitochondria and cellular homeostasis.

Conclusions

Mitochondria represent an ideal environment for post-translational regulation via ADP-ribosylation due to elevated NAD^+ levels, and in fact, several mitochondrial proteins have been recently identified as poly-ADP-ribosylated targets by large-scale proteomic studies (Brunyanszki et al., 2016; Vivelo

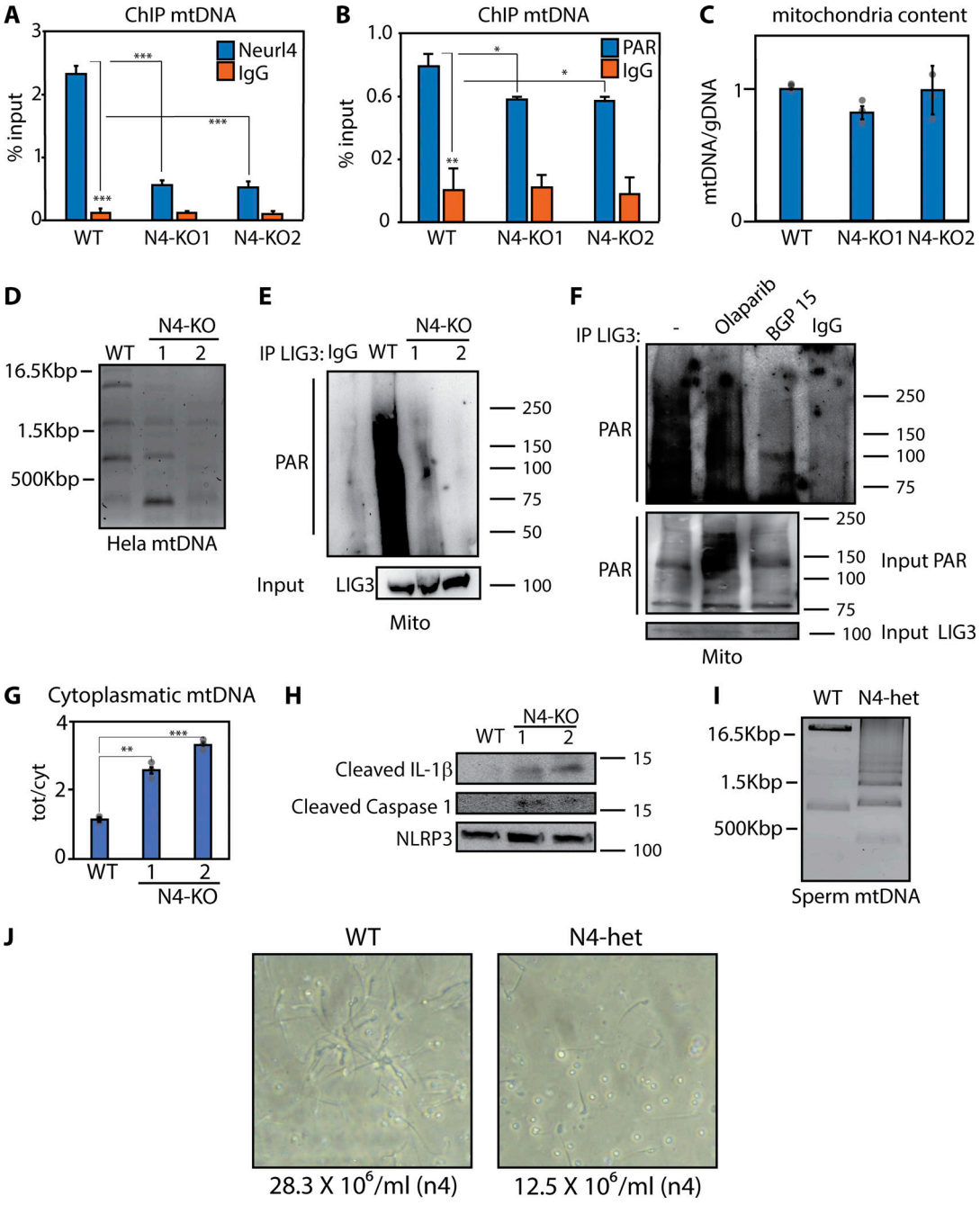

Figure 3. **NEURL4 is required for the regulation of mtDNA integrity. (A and B)** ChIP analysis showing recruitment of NEURL4 at mtDNA sites (A) and decreased levels of poly-ADP-ribosylation associated with mtDNA in N4-KO cells (B). Plots include representative results obtained in three distinct biological replicate experiments, with bar graphs representing the mean ± SD between technical triplicates of one single experiment. **(C)** No significant change in mtDNA copy number as measured by PCR ratio between mtDNA and nuclear DNA. Data represent the mean ± SD of three experiments. **(D)** Long-range PCR assay with Cytb divergent primers showing increased mtDNA deletions in N4-KO cells as compared with the HeLa parental line (WT). **(E and F)** IP assay showing suppression of mtLIG3 PARylation in the absence of NEURL4 (E) or in the presence of the generic PARP inhibitor BGP-15 (F). **(G)** Quantitative PCR assay showing increased mtDNA accumulation in the cytoplasm of N4-KO cells as compared with parental Hela cells. Data represent the mean ± SD of three experiments. **(H)** WB showing activation of caspase 1 and IL-1β in N4-KO cells. **(I)** Long-range PCR assay showing increased mtDNA deletions in spermatocytes from NEURL4$^{+/-}$ mice (N4-het) compared with WT littermates. **(J)** Decreased sperm count in NEURL4 heterozygous mice compared with WT littermates. Mean of sperm count across five random fields for four mice/genotype ± SD. Statistical significance calculated by two-tailed Student's *t* test. *, P < 0.05; **, P < 0.01; ***, P < 0.001. Mito, mitochondrial extracts; tot/cyt, ratio of amplification in total and cytosolic extracts; Cytb, Cytochrome b.

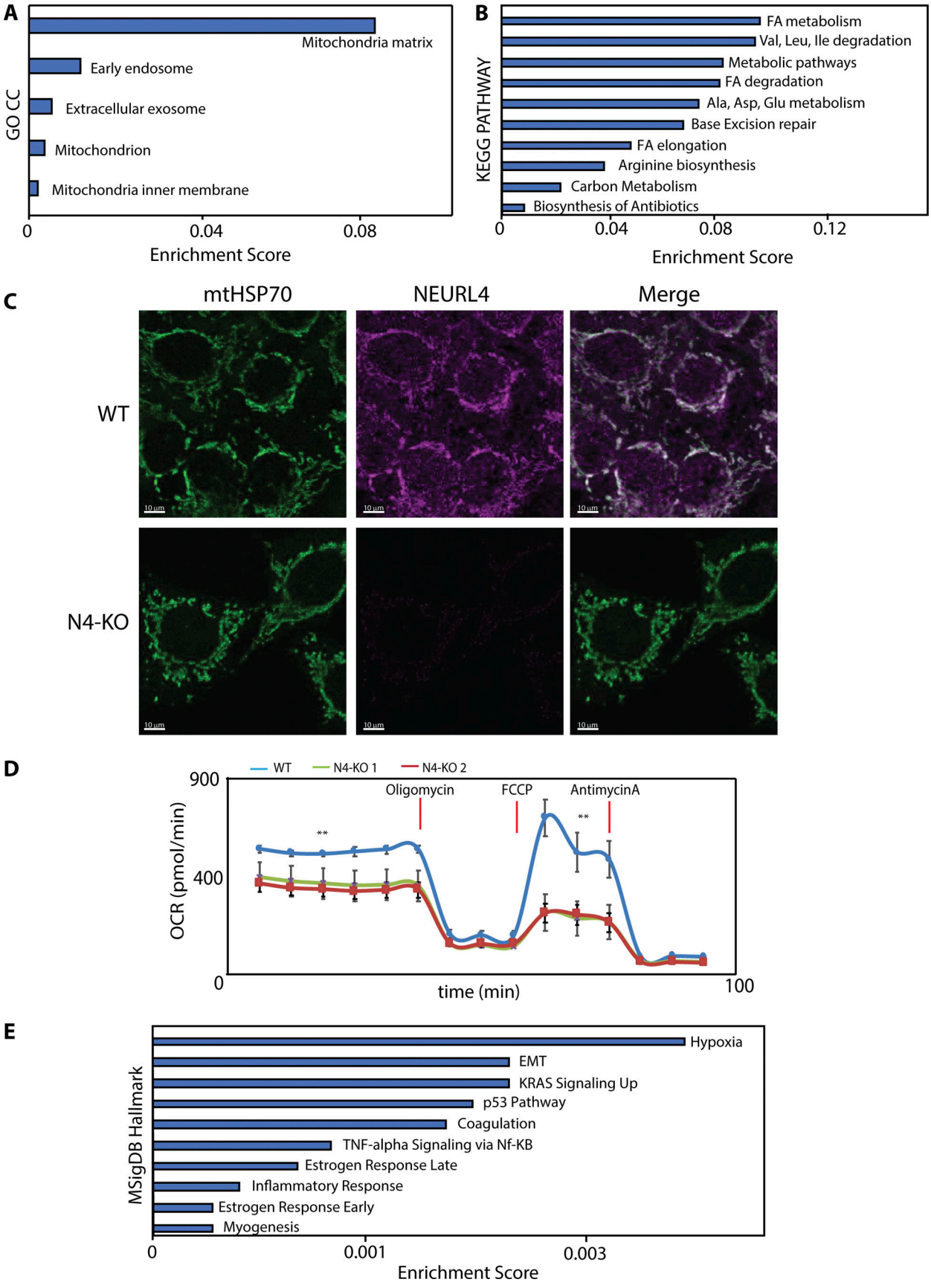

Figure 4. **NEURL4-mediated regulation of mitochondrial proteins by PARylation. (A and B)** SILAC-based enrichment of PARylated proteins in the absence of exogenous genotoxic stress. Most significant gene ontology (GO) terms associated with proteins with decreased PARylation in the absence of NEURL4

(A). Most significant pathways associated with decreased PARylation in the absence of NEURL4 (B). GO terms and KEGG pathways enrichment are based on a combined score between P value and Z score (DAVID). **(C)** Immunostaining showing mitochondrial network changes in HeLa cells in the absence of NEURL4. **(D)** Decreased basal respiration and impaired FCCP response in HeLa N4-KO cells by Seahorse. **(E)** Most significant gene sets from the Molecular Signature Database (MSigDB) enriched among DEGs between WT and N4-KO HeLa cells. CC, cellular components; FA, fatty acid; OCR, oxygen consumption rate; EMT, epithelial-mesenchimal transition; KEGG, Kyoto Encyclopedia of Genes and Genomes; DAVID, Datavase for Annotation, Visualization, and Integrated Discovery.

et al., 2017). However, the ART enzymes that mediate their modifications have remained elusive for a long time (Brunyanszki et al., 2016). Two ARTs enzymes, SIRT4 and PARP1, have been previously reported in mitochondria, but their impact on the mitochondrial PARylome is unclear, with glutamate dehydrogenase being the sole mitochondrial target of SIRT4 identified to date (Herrero-Yraola et al., 2001; Rossi et al., 2009). Here we have characterized NEURL4 as a novel member of the ARTD family (to be named PARP17; Hottiger et al., 2010; Lüscher et al., 2021) and the long-sought ART enzyme responsible of carrying out ADP-ribosylation in the mitochondria. Our results confirm the enzymatic activity of a predicted ARTD-like domain located at the C terminus; characterize NEURL4 presence in the mitochondria matrix, where it interacts with mtDNA; and define the NEURL4-dependent mitochondrial PARylome.

Major conclusions of our work are the confirmation that NEURL4 is an ART enzyme and the characterization of its catalytic domain, which is sufficient for synthesizing PAR chains in vitro. In regard to the nature of the NEURL4-mediated ADP-ribosylation, our data indicate that NEURL4 can support poly-ADP-ribosylation, in agreement with the presence of a conserved E residue in the catalytic domain. However, current results do not exclude the possibility that NEURL4 could mediate MARylation as well, as previously reported for other ARTs (Lüscher et al., 2021). Additional biochemical and structural studies will be necessary to fully uncover the nature of NEURL4 enzymatic activity. In particular, NEURL4 activity appears to be DNA-dependent. Further studies should address the region responsible for interaction with DNA, as well the underlying mechanism of activation. The identification of specific inhibitors against NEURL4 should also be prioritized as critical tools for investigating the biological outcomes of NEURL4 activity in vivo. Intriguingly, our results indicates that ADP-ribosylation in mitochondria is sensitive to BGP-15, a PARP inhibitor with therapeutic potential for treatment of insulin resistance and mitochondria-related diseases. However, it remains unclear whether BGP-15 effects are mediated by direct or indirect modulation of NEURL4 activity.

From a functional point of view, NEURL4 deletion leads to the almost complete loss of PAR synthesis in the mitochondria, in both human and mouse cells. Accordingly, profiling of NEURL4-mediated PARylome by mass spectrometry revealed putative targets implicated in several mitochondrial processes, including metabolites and ions transport, protein synthesis, metabolism, oxidative respiration, and mtDNA repair. Although further studies are needed to elucidate the effect of NEURL4-dependent PARylation on the regulation of each specific target, based on the broad range of mitochondrial functions that are potentially regulated by NEURL4-dependent ADP-ribosylation, we expect that NEURL4 plays a prominent role in the regulation of mitochondrial functions. Indeed, NEURL4-KO cells present a severe mitochondrial phenotype. Not only do mitochondria appear stressed, with loss of mitochondrial membrane potential and impaired mtDNA integrity, but the cells also undergo a global gene expression reprogramming that reflects the dysregulations of some of the enzymes identified as potential targets. For example, dysregulation of inflammatory pathways reflected the increase in mtDNA-driven activation of danger-associated molecular pattern signaling upon release of mtDNA in the cytosol due to defective regulation of mtLIG3. Our data, in fact, indicate that loss of mtLIG3 PARylation, in the absence of NEURL4, correlates with decreased mtDNA stability, elevated mtDNA levels in the cytosol, and corresponding activation of an innate immune response leading to increased IL-1β processing. NEURL4 relevance for the maintenance of mtDNA integrity was confirmed in vivo as the spermatocytes of male NEURL4$^{+/-}$ heterozygous mice show significant accumulation of mtDNA deletions, which leads to reduced sperm count and increased agglutination. Remarkably, de novo mutations in the *Neurl4* gene were recently identified as causative of human male infertility (Hodžić et al., 2021), in agreement with extensive literature linking mtDNA deletions with infertility in both mice and humans (Jiang et al., 2017; Karimian and Babaei, 2020; Kumar and Sangeetha, 2009). On the contrary, PARP1-KO mice show no major phenotypic differences when compared with WT, unless under genotoxic stress (Niere et al., 2008). Additionally, the N4-KO signature is characterized by the activation of p53-related pathways. One of the triggers of p53 activation is the decrease in pyrimidine synthesis (Khutornenko, 2010), which is regulated by CPS1, another validated NEURL4 target.

While more work is required to confirm NEURL4 individual targets, determine the specific modification sites on target proteins, and assess the effect of ADP-ribosylation on proteins' function, it is important to note that the transcriptomic, morphological, and functional changes observed in NEURL4-null cells are opposite from those induced by the depletion of PARP1 (Módis et al., 2012; Niere et al., 2008), thus reaffirming that the observed phenotypes are specific to NEURL4 deletion and further highlighting the pivotal role of NEURL4 in the maintenance of mitochondrial homeostasis under physiological conditions (Fig. 5).

Materials and methods

Experimental model and subject details

HeLa cells were grown in 10% FBS/DMEM supplemented with 0.1 mM MEM nonessential aa, 2 mM L-glutamine, and 1 mM sodium pyruvate. For cell transfection, Lipofectamine 2000 was used following the manufacturer's protocol (Invitrogen). 1 µM olaparib (Cell Signaling), 10 µg/ml BGP-15, and 10 µM FCCP

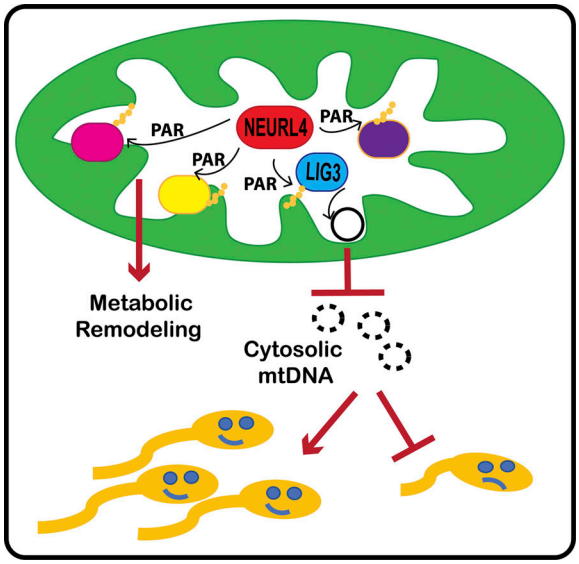

Figure 5. **Model for NEURL4-mediated regulation of mitochondria homeostasis and male infertility.**

(TOCRIS) were used for cell treatments. Two NEURL4 KO cell lines (N4-KO1 and N4-KO2) were generated using standard CRISPR/Cas9 genome editing technology with two independent single guide RNAs (sgRNAs; gRNA-NEURL4-exon15 sequence forward 5′-CACCGACATAGTCACCTTTACCCGG-3′ and reverse 5′-AAACCCGGGTAAAGGTGACTATGTC-3′; gRNA-NEURL4-exon2 sequence forward 5′-CACCGCTTGCCATAAAGGTCCACG A-3′ and reverse 5′-AAACTCGTGGACCTTTATGGCAAGC-3′). NEURL4 heterozygote mice were generated by the Boston Nutrition Obesity Research Center Transgenic Core via injection of NEURL4 KO embryonic stem (ES) cells purchased from the Knockout Mouse Project (KOMP) repository. Mice were maintained on a standard laboratory chow diet in a temperature-controlled facility on a 12-h light/dark cycle. All animal studies were approved by the Boston University Institutional Animal Care and Use Committee and performed in strict accordance with National Institutes of Health guidelines for animal care.

Cell staining

Immunostaining was performed following standard protocols on cells fixed in 4% paraformaldehyde/PBS using Rhodamine RedX–conjugated secondary antibodies anti-rabbit (Jackson ImmunoResearch; 711–295-152) and FITC-conjugated secondary antibodies anti-mouse (Jackson ImmunoResearch; 715–095-151), and ATP5B mouse monoclonal (Molecular Probes; A21351) and NEURL4 rabbit polyclonal ct (custom aa 1492–1508) as primary antibodies. Single-focal-plane images were acquired with a 40× oil lens (NA 1.4) and were captured using a Zeiss LMS 700 Laser confocal microscope couple with an ERC5 camera via ZEISS ZEN software (FITC [488 nm], Cy5 [639 nm]). Images were then processed for publication using ImageJ. Controls slides, incubated only with secondary antibodies, were processed for each sample. Merging of the immunostaining signal from different antibodies was used as an indication of proteins colocalization in a specific cellular compartment.

Recombinant protein expression

Human NEURL4 cDNAs encoding either the NEURL4-Ct domain WT or mutant (HGS to AGA and ELEW to ALAA) were subcloned into pET-32a-His-tag expression vectors. Proteins were produced in BL21 *E. coli*, resin-purified on nickel-nitrilotriacetic acid beads, and eluted according to the manufacturer's protocol (Life Technologies). The His-NEURL4-Ct–conjugated agarose was stored at 4°C in PBS supplemented with 30% glycine.

Purified GST-tagged WWE domain was obtained by expressing the proteins in *E. coli* BL21(DE3) cells, which were induced with 0.5 mM isopropyl 1-thio-β-D-galactopyranoside for 4 h at 30°C. The harvested cells were lysed by sonication in lysis buffer (1 mM DTT and 1% Triton X-100 in PBS). GST-WWE fusion protein was purified from cell lysates using glutathione-Sepharose 4B beads (Qiagen) according to the manufacturer's instructions. The GST-WWE–conjugated agarose was stored at 4°C in PBS supplemented with 30% glycine.

Protein extraction, subcellular fractionation, submitochondrial localization, and IP

For whole-cell extract preparation, cells were rinsed in PBS, harvested, and incubated for 20 min on ice in IPH buffer (50 mM Tris-HCl, pH 8.0, 150 mM NaCl, 5 mM EDTA, 0.5% NP-40, 50 mM NaF, 2 mM Na_2VO_3, 1 mM PMSF, and protease inhibitor mix). For cytoplasmatic, mitochondrial, and nuclear extracts fractionation, cells were rinsed in PBS, harvested, and resuspended in gradient buffer (10 mM Hepes, pH 7.9, 1 mM EDTA, 210 mM mannitol, 70 mM sucrose, 10 mM N-ethylmalemide (NEM), 50 mM NaF, 2 mM Na_2VO_3, 1 mM PMSF, and protease inhibitors cocktail), then homogenized via 10 passages through a 25-G syringe followed by low-speed centrifugation for 10 min. The nuclear pellet was incubated for 20 min in high-salt buffer (10 mM Hepes, pH 7.9, 20% glycerol, 420 mM NaCl, 1.5 mM $MgCl_2$, 0.2 mM EDTA, 0.5 mM DTT, 10 mM NEM, 50 mM NaF, 2 mM Na_2VO_3, 1 mM PMSF, and protease inhibitor mix) while the supernatant was recovered and subjected to high-speed centrifugation to separate the mitochondrial pellet from the cytoplasmic fraction. The mitochondrial pellet was incubated for 15 min in lysis buffer (50 mM Tris-HCl, pH 8, 300 mM NaCl, 1 mM EDTA, 1% Triton X-100, 10 mM NEM, 50 mM NaF, 2 mM Na_2VO_3, 1 mM PMSF, and protease inhibitor mix). Blotting with markers of the different fractions (HDAC2 rabbit polyclonal for nuclear extract from Santa Cruz, H-54 sc7899; mtHSP70 mouse monoclonal for mitochondrial extracts and mitochondrial matrix from Enzo, JG1 ALX-804-077-R100; TOM20 mouse monoclonal for outer mitochondrial membrane from Santa Cruz, F-10 sc-17764; AIF mouse monoclonal from Santa Cruz, E-11 sc-390619, for inner mitochondrial membrane; and β-tubulin mouse monoclonal from Sigma-Aldrich, D66 T0198 for cytoplasmatic extract) was used to assess purity. Poly-(ADP-ribose) polyclonal rabbit antibody (Enzo Life Science; ALX-210-890A) was used to test PARylation level. Flag-HRP (Sigma-Aldrich; A8592) for detection of FLAG-tagged proteins. To examine submitochondrial localization, the isolated mitochondria fraction was treated with either proteinase K (2, 5, or 10 ng) in ice for 30 min or 50 µg/ml trypsin on ice for 30 min under either isotonic or hypotonic conditions. The

reaction was terminated by adding, respectively, 1 mM PMSF or 10% TCA. Concentration of protein extracts was measured using the colorimetric Bio-Rad assay. Extracts were boiled in SDS sample buffer and loaded onto 10% Mini-PROTEAN TGX gels (Bio-Rad), before transfer onto PVDF membranes (Millipore) and WB following standard protocols. For IP, cells were transfected with FLAG-NEURL4-DCt or FLAG-NEURL4-Ct. Then mitochondria were isolated and protein extract incubated with the anti-FLAG agarose beads (Millipore Sigma; A4596) overnight at 4°C, washed extensively, and stored at 4°C in PBS supplemented with 30% glycine.

In vitro PARylation assay

IP NEURL4 protein or recombinant NEURL4-Ct protein was incubated with Biot-NAD^+ (TOCRIS; 6573) in reaction buffer (50 mM Tris-HCl, pH 7.4, and 2 mM $MgCl_2$) with or without 2.5 µg of single strand DNA (ssDNA; Sigma-Aldrich) at 37°C for 30 min. The reaction was stopped by adding 2X Laemmli sample buffer (Bio-Rad; 1610737). Reactions were loaded on 15–4% gradient Mini-PROTEAN TGX gels (Bio-Rad) before transfer onto PVDF membranes (Millipore) and WB following standard protocols with streptavidin-HRP (Thermo Fisher Scientific; SA10001) to monitor PARylation levels. Olaparib and BGP15 were added at the beginning of the 30-min reaction.

ChIP assay

For ChIP, ~10^7 cells were cross-linked with 1% formaldehyde at room temperature (~25°C) for 10 min and neutralized with 0.125 M glycine. Mitochondria were isolated using the protocol described above and then lysed in lysis buffer for 10 min at 4°C. Lysates were sonicated using a Diogenode Bioraptor Sonicator with a Diagenode-compatible 1.5-ml Micro Tube for four cycles, 10 s on and 40 s off at maximum power. Debris was removed by centrifugation for 10 min at 13,000 rpm at 4°C, and sonication was checked via DNA electrophoresis. After diluting supernatant fraction 10-fold in ChIP Dilution Buffer (0.01% SDS, 1.1% Triton X-100, 1.2 mM EDTA, 16.7 mM Tris-HCl, pH 8, and 167 mM NaCl with protease inhibitors), chromatin was incubated with 2 µg antibody or IgG control at 4°C overnight (NEURL4 rabbit polyclonal ct custom aa 1492–1508 or PAR polyclonal rabbit, Enzo Life Science; ALX-210-890A). IP complexes were collected using Sepharose A beads (Life Technologies). Beads were pelleted by centrifugation for 1 min at 1,000 rpm and washed four times with 500 µl of, respectively, Low Salt Wash Buffer (150 mM NaCl, 20 mM Tris-HCl, pH 8.0, 2 mM EDTA, 1% Triton X-100, and 0.1% SDS), High Salt Wash Buffer (500 mM NaCl, 20 mM Tris-HCl, pH 8.0, 2mM EDTA, 1% Triton X-100, and 0.1% SDS), LiCl Wash (0.25 M LiCl, 10 mM Tris-HCl, pH 8.0, 1 mM EDTA, 1% Igepal, and 1% deoxycholate), and 1X Tris-EDTA (1 M Tris-HCl, pH 8.0, 10 mM EDTA) using the Centrifugal Filter Units Durapore PVDF 0.45 µm (Millipore). DNA was extracted and purified by phenol/chloroform extraction. Quantitative PCR was performed using specific primers against human mitochondrial-encoded NADH dehydrogenase 1 (mt-ND1) locus (forward 5′-CAACCCCCTGGTCAACCTCA-3′ and reverse 5′-GCC GATCAGGGCGTAGTTTG-3′). ChIP experiments were repeated at least three times, and representative results are shown as samples mean between technical replicates ± SD. Significance was calculated by paired Student's *t* test.

RNA isolation, RT-PCR analysis, and RNA-seq

RNA was isolated from cell or mouse tissue following the manufacturer's protocol for the RNeasy Kit (Qiagen). For the RNA-seq, cells were subjected to standard RNA isolation before RNA library preparation following Illumina's RNA-Seq Sample Preparation Protocol. Resulting cDNA libraries were sequenced on the Illumina HiSeq 2000. Data have been deposited in GEO under accession no. GSE183952.

Immunogold EM

For preparation of cryosections, cells were rinsed in PBS, harvested, and fixed in 4% paraformaldehyde/PBS for 2 h. Then cells were infiltrated with 2.3 M sucrose/PBS/0.2 M glycine) and frozen in liquid nitrogen. Frozen samples were sectioned at −120°C and transferred to formvar-carbon–coated copper grids. Grids were floated on PBS or put on 2% gelatin dishes in the refrigerator until the immunogold labeling was performed. The gold labeling was performed at room temperature on a piece of parafilm. All antibodies and protein A gold were diluted in 1% BSA in PBS. The diluted antibody solution was centrifuged 1 min at 14,000 rpm before labeling to avoid possible aggregates. Grids were floated on drops of 1% BSA for 10 min to block for unspecific labeling, transferred to 5-µl drops of primary antibody, and incubated for 30 min. The grids were then washed in four drops of PBS for a total of 15 min, transferred to 5-µl drops of Protein-A gold for 20 min, and washed in four drops of PBS for 15 min and six drops of double-distilled water. Contrasting/embedding of the labeled grids was performed on ice in 0.3% uranyl acetate in 2% methyl cellulose for 10 min. Grids were picked up with metal loops (diameter slightly larger than the grid), and the excess liquid was removed by streaking on a filter paper (Whatman #1), leaving a thin coat of methyl cellulose (bluish interference color when dry). Control grids without primary antibody, incubated only with Protein-A gold, were processed for each sample (Harvard EM Core standard protocols). The grids were examined in a JEOL 1200EX Transmission electron microscope, and images were recorded with an AMT 2k CCD camera with a direct magnification of 15,000×.

Mitochondrial content, mtDNA cytoplasmic content, and long-range PCR

Total DNA was extracted from cells using QuickExtract DNA Extraction Solution 1.0 (Epicenter) following the manufacturer's instructions. To isolate DNA from the cytoplasm cell pellets were resuspended in 500 µl buffer composed of 150 mM NaCl, 50 mM Hepes, pH 7.4, and 25 mg/ml digitonin. The homogenates were mixed for 10 min at room temperature to allow plasma membrane permeabilization, then centrifuged at 1,000 *g* for 10 min to pellet intact cells. Cytosol-containing supernatant was transferred to a new tube and centrifuged at 17,000 *g* for 10 min to remove any remaining cellular debris. DNA was then isolated from this fraction using the DNA purification kit from Qiagen. Quantitative PCR was performed on whole-cell extracts and cytosolic fractions using mt-ND1 relative to nuclear

transcription factor A, mitochondrial (TFAM) to determine mitochondrial DNA copy numbers (human mt-ND1 primers forward 5′-CAACCCCCTGGTCAACCTCA-3′ and reverse 5′-GCC GATCAGGGCGTAGTTTG-3′; human TFAM primers forward 5′-TGCTTGGAAAACCAAAAAGACCTC-3′ and reverse 5′-TGAATC ACCCTTAGCTTCTTGGAA-3′; mouse mt-ND1 primers forward 5′-GCCACCTTACAAATAAGCGCTCTC-3′ and reverse 5′-ACG CAATTTCCTGGCTCTGC-3′; and mouse TFAM primers forward 5′-CTGCACTCTGCCCATCCAAA-3′ and reverse 5′-CTGAGCATT CGCAGGCCTTT-3′). Long Range PCR to amplify the entire mtDNA was performed using Long Amp Hot Start Taq DNA Polymerases (NEB) according to the manufacturer's protocol using Cytb divergent primers (human forward 5′-TGAGGCCAA ATATCATTCTGAGGGGC-3′ and reverse 5′-TTTCATCATGCG GAGATGTTGGATGG-3′; mouse forward 5′-GACGTAAATTAC GGTGACTA-3′ and reverse 5′-TAGTCACCCGGTAATTTACGT C-3′).

Respirometry

Cells were plated in Seahorse V.7 multi-well culture plates. The next day, media were replaced by running media (XF Seahorse Assay Media supplemented with 5.5 mM glucose, 0.5 mM pyruvate, and 1 mM glutamine), and the plate was placed in the incubator at 37°C for 1 h (no carbon dioxide). Oxygen consumption was measured at 37°C using a Seahorse XF24 Extracellular Flux Analyzer (Seahorse Bioscience). Mitochondrial stress test compounds (10 µM oligomycin, 2.5 µM FCCP, and 10 µM antimycin A) were injected through ports A, B, and C, respectively, to measure mitochondrial respiration linked to ATP synthesis, leak, maximal respiratory capacity, and nonmitochondrial oxygen consumption according to the manufacturer's instructions.

SILAC-based mitochondrial poly-ADP-ribosylation proteins pull-down and in-gel digestion

For SILAC experiments, HeLa cells were grown in medium containing unlabeled L-arginine and L-lysine (Arg^0/Lys^0) as the light condition, or isotope-labeled variants of L-arginine and L-lysine (Arg^{10}/Lys^8) as the heavy condition. For pull-down of poly-ADP-ribosylation proteins, mitochondrial proteins were extracted from SILAC-labeled HeLa WT and Neurl4-KO cells as described before. GST-WWE–conjugated agarose was added to immobilize the poly-ADP-ribosylation proteins using equal amounts of proteins from the two SILAC states and incubating at 4°C for 1 h; bound material was washed extensively in high-stringency buffer (50 mM Tris-HCl, pH 7.5, 500 mM NaCl, 5 mM EDTA, 1% NP-40, 1 mM DTT, and 0.1% SDS). Proteins were separated by SDS-PAGE and visualized with Coomassie blue stain, and then were digested in-gel by trypsin overnight. The resulting peptides were desalted using C18 Tips (Thermo Fisher Scientific) per the manufacturer's instructions.

Mass-spectrometric analysis

Peptides were analyzed on a Q-Exactive HF mass spectrometer (Thermo Fisher Scientific) equipped with a nanoflow HPLC system (Thermo Fisher Scientific). Peptides were loaded onto a C18 trap column (3 µm, 75 µm × 2 cm; Thermo Fisher Scientific) connected in-line to a C18 analytical column (2 µm, 75 µm × 50 cm; Thermo EasySpray) using the Thermo EasyLC 1200 system with the column oven set to 55°C. The nanoflow gradient consisted of buffer A (composed of 2% [vol/vol] ACN with 0.1% Q:35 formic acid) and buffer B (consisting of 80% (vol/vol) ACN with 0.1% formic acid). For protein analysis, nanoflow HPLC was performed for 180 min at a flow rate of 250 nl/min, with gradient steps as follows: 2–8% B for 5 min, 8–20% B for 96 min, 20–35% B for 56 min, 35–98% B for 3 min, 98% buffer B for 3 min, 100% B for 3 min, 5% B for 14 min. Peptides were directly ionized using a nanospray ion source into a Q-Exactive HF mass spectrometer (Thermo Fisher Scientific).

The Q-Exactive HF was run using data-dependent acquisition, ions were analyzed by mass spectrometry (MS1), with the top 10 most intense ions serially selected for higher-energy C-trap dissociation (HCD) fragmentation and analysis by a second stage of mass spectrometry (MS2). Full MS1 spectra were collected at a resolution of 120,000 with an automatic gain control (AGC) target of 3e6, maximum injection time of 60 ms, and scan range of 350 to 1,650 m/z. MS2 scans were performed at 45,000 resolution with an AGC target 2e4, maximum injection time of 90 ms, using 33% normalized collision energy (NCE). Source ionization parameters were optimized with the spray voltage at 2.1 kV, transfer temperature at 275°C. Dynamic exclusion was set to 40 s.

Data analysis

All acquired MS/MS spectra were searched against the Uniprot human complete proteome FASTA database downloaded on October 26, 2018, using the MaxQuant software (version 1.6.7.0) that integrates the Andromeda search engine. Enzyme specificity was set to trypsin, and up to two missed cleavages were allowed. Cysteine carbamidomethylation was specified as a fixed modification. Methionine oxidation, N-terminal acetylation, and ADP-ribosylation on a wide range of aa residues (C, D, E, H, K, R, S, T, and Y) were included as variable modifications. Peptide precursor ions were searched with a maximum mass deviation of 6 ppm and fragment ions with a maximum mass deviation of 20 ppm. Peptide and protein identifications were filtered at 1% false discovery rate using the target-decoy database search strategy. Proteins that could not be differentiated based on MS/MS spectra alone were grouped to protein groups (default MaxQuant settings). Data are available via ProteomeXchange with identifier PXD029538.

Statistical analysis

All data shown in the histograms are the results of at least three independent experiments and are presented as the mean ± SEM. Hand ChIPs data are representative of three independent experiments, and bar graphs represent the sample mean of three technical replicates ± SD. The differences between groups were compared using two-tailed Student's *t* test assuming that data distribution was normal, but this was not formally tested. Imaging results and WB are representative of three independent experiments.

Online supplemental material

Fig. S1, a supplement to Fig. 2, shows total acetylation changes in NEURL4 WT and KO cells. Fig. S2, a supplement to Fig. 4, shows additional alayses of proteomics and genomics data. Video 1 (WT

sperm) is time-lapse epifluorescence microscopy showing WT mice normal sperm movement. Video 2 (KO sperm) is time-lapse epifluorescence microscopy showing increased sperm agglutination for NEURL4$^{+/-}$ heterozygous mice. Table S1 shows raw proteomic data and the list of potential NEURL4 targets. Table 2 shows the list of differentially expressed genes between NEURL4 WT and KO cells.

Data availability

Requests for further information may be directed to and will be fulfilled by the lead contacts, M.D. Cardamone (dafne.cardamone@hotmail.com) and V. Perissi (vperissi@bu.edu).

Acknowledgments

We are grateful to past and present members of the Perissi laboratory and to Dr. Marc Liesa (University of California, Los Angeles) for feedback and stimulating discussions, and to Dr. L. Aravind for sharing useful insights about the predicted enzymatic activity of NEURL4. We thank Dr. Wenqing Xu (University of Washington), Seattle, WA for sharing the construct for expressing the Rnf146 WWE domain. We are thankful for the excellent assistance provided by the Boston University School of Medicine (BUSM) Microarray and Sequencing Core Facility (Dr. Yuriy Alekseyev), the BUSM Confocal Microscopy Facility (Dr. Vickery Trinkaus-Randall), the BUSM Analytical Instrumentation Core (Dr. Lynn Deng), the Boston Nutrition Obesity Research Center (BNORC) Adipose Biology and Metabolism Core (Dr. Stephen Farmer) and Mouse Transgenic Core (Dr. Brad Lowell), and the Harvard Electron Microscopy Facility (Dr. Maria Ericsson).

This work was supported by the National Institutes of Health (R01DK100422 and R01GM127625) to V. Perissi, a Pilot and Feasibility Award to M.D. Cardamone from the BNORC (P30DK046200), and a Grunebaum Cancer Foundation Fellowship to M.D. Cardamone.

The authors declare no competing financial interests.

Author contributions: M.D. Cardamone and V. Perissi conceived and planned the experiments, interpreted the results, and wrote the manuscript with help and critical feedback from all other authors. M.D. Cardamone carried out all the biochemistry-based, cell-based, and animal-based experiments with assistance from Y. Gao, V. Hayashi, M. Sheeran, and J. English. M.D. Cardamone and Y. Gao prepared samples for the omics profiling experiments. J. Kwan performed and analyzed all mass spectrometry experiments under the supervision of A. Emili. J. Xu and J. Orofino performed the analysis of transcriptomics data.

Submitted: 5 January 2021
Revised: 7 September 2021
Accepted: 4 November 2021

References

Al-Hakim, A.K., M. Bashkurov, A.C. Gingras, D. Durocher, and L. Pelletier. 2012. Interaction proteomics identify NEURL4 and the HECT E3 ligase HERC2 as novel modulators of centrosome architecture. *Mol. Cell. Proteomics.* 11:014233. https://doi.org/10.1074/mcp.M111.014233

Altmeyer, M., S. Messner, P.O. Hassa, M. Fey, and M.O. Hottiger. 2009. Molecular mechanism of poly(ADP-ribosyl)ation by PARP1 and identification of lysine residues as ADP-ribose acceptor sites. *Nucleic Acids Res.* 37:3723–3738. https://doi.org/10.1093/nar/gkp229

Amé, J.C., C. Spenlehauer, and G. de Murcia. 2004. The PARP superfamily. *BioEssays.* 26:882–893. https://doi.org/10.1002/bies.20085

Aravind, L., D. Zhang, R.F. de Souza, S. Anand, and L.M. Iyer. 2015. The natural history of ADP-ribosyltransferases and the ADP-ribosylation system. *Curr. Top. Microbiol. Immunol.* 384:3–32.

Azarm, K., and S. Smith. 2020. Nuclear PARPs and genome integrity. *Genes Dev.* 34:285–301. https://doi.org/10.1101/gad.334730.119

Bai, P., and C. Cantó. 2012. The role of PARP-1 and PARP-2 enzymes in metabolic regulation and disease. *Cell Metab.* 16:290–295. https://doi.org/10.1016/j.cmet.2012.06.016

Barkauskaite, E., G. Jankevicius, and I. Ahel. 2015. Structures and Mechanisms of Enzymes Employed in the Synthesis and Degradation of PARP-Dependent Protein ADP-Ribosylation. *Mol. Cell.* 58:935–946. https://doi.org/10.1016/j.molcel.2015.05.007

Bonfiglio, J.J., P. Fontana, Q. Zhang, T. Colby, I. Gibbs-Seymour, I. Atanassov, E. Bartlett, R. Zaja, I. Ahel, and I. Matic. 2017. Serine ADP-Ribosylation Depends on HPF1. *Mol. Cell.* 65:932–940.e6. https://doi.org/10.1016/j.molcel.2017.01.003

Brunyanszki, A., B. Szczesny, L. Virág, and C. Szabo. 2016. Mitochondrial poly(ADP-ribose) polymerase: The Wizard of Oz at work. *Free Radic. Biol. Med.* 100:257–270. https://doi.org/10.1016/j.freeradbiomed.2016.02.024

Burzio, L.O., L. Sáez, and R. Cornejo. 1981. Poly (ADP-ribose) synthetase activity in rat testis mitochondria. *Biochem. Biophys. Res. Commun.* 103:369–375. https://doi.org/10.1016/0006-291X(81)91702-2

Claros, M.G. 1995. MitoProt, a Macintosh application for studying mitochondrial proteins. *Comput. Appl. Biosci.* 11:441–447. https://doi.org/10.1093/bioinformatics/11.4.441

Cohen, M.S., and P. Chang. 2018. Insights into the biogenesis, function, and regulation of ADP-ribosylation. *Nat. Chem. Biol.* 14:236–243. https://doi.org/10.1038/nchembio.2568

Cubillos-Rojas, M., T. Schneider, R. Bartrons, F. Ventura, and J.L. Rosa. 2017. NEURL4 regulates the transcriptional activity of tumor suppressor protein p53 by modulating its oligomerization. *Oncotarget.* 8:61824–61836. https://doi.org/10.18632/oncotarget.18699

DaRosa, P.A., Z. Wang, X. Jiang, J.N. Pruneda, F. Cong, R.E. Klevit, and W. Xu. 2015. Allosteric activation of the RNF146 ubiquitin ligase by a poly(ADP-ribosyl)ation signal. *Nature.* 517:223–226. https://doi.org/10.1038/nature13826

de Souza, R.F., and L. Aravind. 2012. Identification of novel components of NAD-utilizing metabolic pathways and prediction of their biochemical functions. *Mol. Biosyst.* 8:1661–1677. https://doi.org/10.1039/c2mb05487f

Ding, W.X., M. Li, J.M. Biazik, D.G. Morgan, F. Guo, H.M. Ni, M. Goheen, E.L. Eskelinen, and X.M. Yin. 2012. Electron microscopic analysis of a spherical mitochondrial structure. *J. Biol. Chem.* 287:42373–42378. https://doi.org/10.1074/jbc.M112.413674

Fehr, A.R., S.A. Singh, C.M. Kerr, S. Mukai, H. Higashi, and M. Aikawa. 2020. The impact of PARPs and ADP-ribosylation on inflammation and host-pathogen interactions. *Genes Dev.* 34:341–359. https://doi.org/10.1101/gad.334425.119

Grazioli, S., and J. Pugin. 2018. Mitochondrial damage-associated molecular patterns: From inflammatory signaling to human diseases. *Front. Immunol.* 9:832. https://doi.org/10.3389/fimmu.2018.00832

Gupte, R., Z. Liu, and W.L. Kraus. 2017. PARPs and ADP-ribosylation: recent advances linking molecular functions to biological outcomes. *Genes Dev.* 31:101–126. https://doi.org/10.1101/gad.291518.116

Hassler, M., and A.G. Ladurner. 2012. Towards a structural understanding of PARP1 activation and related signalling ADP-ribosyl-transferases. *Curr. Opin. Struct. Biol.* 22:721–729. https://doi.org/10.1016/j.sbi.2012.08.005

Hendriks, I.A., S.C. Larsen, and M.L. Nielsen. 2019. An Advanced Strategy for Comprehensive Profiling of ADP-ribosylation Sites Using Mass Spectrometry-based Proteomics. *Mol. Cell. Proteomics.* 18:1010–1026. https://doi.org/10.1074/mcp.TIR119.001315

Herrero-Yraola, A., S.M.A. Bakhit, P. Franke, C. Weise, M. Schweiger, D. Jorcke, and M. Ziegler. 2001. Regulation of glutamate dehydrogenase by reversible ADP-ribosylation in mitochondria. *EMBO J.* 20:2404–2412. https://doi.org/10.1093/emboj/20.10.2404

Hodžić, A., A. Maver, D. Plaseska-Karanfilska, M. Ristanović, P. Noveski, B. Zorn, M. Terzic, T. Kunej, and B. Peterlin. 2021. De novo mutations in idiopathic male infertility—A pilot study. *Andrology.* 9:212–220. https://doi.org/10.1111/andr.12897

Hottiger, M.O., P.O. Hassa, B. Lüscher, H. Schüler, and F. Koch-Nolte. 2010. Toward a unified nomenclature for mammalian ADP-

ribosyltransferases. *Trends Biochem. Sci.* 35:208–219. https://doi.org/10.1016/j.tibs.2009.12.003

Imai, Y., Y. Kobayashi, T. Inoshita, H. Meng, T. Arano, K. Uemura, T. Asano, K. Yoshimi, C.L. Zhang, G. Matsumoto, et al. 2015. The Parkinson's Disease-Associated Protein Kinase LRRK2 Modulates Notch Signaling through the Endosomal Pathway. *PLoS Genet.* 11:e1005503. https://doi.org/10.1371/journal.pgen.1005503

Jiang, M., T.E.S. Kauppila, E. Motori, X. Li, I. Atanassov, K. Folz-Donahue, N.A. Bonekamp, S. Albarran-Gutierrez, J.B. Stewart, and N.G. Larsson. 2017. Increased Total mtDNA Copy Number Cures Male Infertility Despite Unaltered mtDNA Mutation Load. *Cell Metab.* 26:429–436.e4. https://doi.org/10.1016/j.cmet.2017.07.003

Jones, J., and P.M. Macdonald. 2015. Neurl4 contributes to germ cell formation and integrity in Drosophila. *Biol. Open.* 4:937–946. https://doi.org/10.1242/bio.012351

Kadam, A., T. Jubin, R. Roychowdhury, and R. Begum. 2020. Role of PARP-1 in mitochondrial homeostasis. *Biochim. Biophys. Acta, Gen. Subj.* 1864: 129669. https://doi.org/10.1016/j.bbagen.2020.129669

Karimian, M., and F. Babaei. 2020. Large-scale mtDNA deletions as genetic biomarkers for susceptibility to male infertility: A systematic review and meta-analysis. *Int. J. Biol. Macromol.* 158:85–93. https://doi.org/10.1016/j.ijbiomac.2020.04.216

Khutornenko. 2010. Pyrimidine biosynthesis links mitochondrial respiration to the p53 pathway. *Proceedings of the National Academy of Sciences*. 107: 12828–12833. https://doi.org/10.1073/pnas.0910885107

Kraus, W.L. 2015. PARPs and ADP-Ribosylation: 50 Years ... and Counting. *Mol. Cell.* 58:902–910. https://doi.org/10.1016/j.molcel.2015.06.006

Kumar, D.P., and N. Sangeetha. 2009. Mitochondrial DNA mutations and male infertility. *Indian J. Hum. Genet.* 15:93–97. https://doi.org/10.4103/0971-6866.60183

Kun, E., P.H. Zimber, A.C.Y. Chang, B. Puschendorf, and H. Grunicke. 1975. Macromolecular enzymatic product of NAD+ in liver mitochondria. *Proc. Natl. Acad. Sci. USA.* 72:1436–1440. https://doi.org/10.1073/pnas.72.4.1436

Leslie Pedrioli, D.M., M. Leutert, V. Bilan, K. Nowak, K. Gunasekera, E. Ferrari, R. Imhof, L. Malmström, and M.O. Hottiger. 2018. Comprehensive ADP-ribosylome analysis identifies tyrosine as an ADP-ribose acceptor site. *EMBO Rep.* 19:e45310. https://doi.org/10.15252/embr.201745310

Leung, A.K. 2014. Poly(ADP-ribose): an organizer of cellular architecture. *J. Cell Biol.* 205:613–619. https://doi.org/10.1083/jcb.201402114

Li, J., S. Kim, T. Kobayashi, F.X. Liang, N. Korzeniewski, S. Duensing, and B.D. Dynlacht. 2012. Neurl4, a novel daughter centriole protein, prevents formation of ectopic microtubule organizing centres. *EMBO Rep.* 13: 547–553. https://doi.org/10.1038/embor.2012.40

Liu, S., and G.L. Boulianne. 2017. The NHR domains of Neuralized and related proteins: Beyond Notch signalling. *Cell. Signal.* 29:62–68. https://doi.org/10.1016/j.cellsig.2016.10.004

Liu, X., and G. Hajnóczky. 2011. Altered fusion dynamics underlie unique morphological changes in mitochondria during hypoxia-reoxygenation stress. *Cell Death Differ.* 18:1561–1572. https://doi.org/10.1038/cdd.2011.13

Loukil, A., K. Tormanen, and C. Sütterlin. 2017. The daughter centriole controls ciliogenesis by regulating Neurl-4 localization at the centrosome. *J. Cell Biol.* 216:1287–1300. https://doi.org/10.1083/jcb.201608119

Lüscher, B., I. Ahel, M. Altmeyer, A. Ashworth, P. Bai, P. Chang, M. Cohen, D. Corda, F. Dantzer, M.D. Daugherty, et al. 2021. ADP-ribosyltransferases, an update on function and nomenclature. *FEBS J.*:febs.16142. https://doi.org/10.1111/febs.16142

Martello, R., M. Leutert, S. Jungmichel, V. Bilan, S.C. Larsen, C. Young, M.O. Hottiger, and M.L. Nielsen. 2016. Proteome-wide identification of the endogenous ADP-ribosylome of mammalian cells and tissue. *Nat. Commun.* 7:12917. https://doi.org/10.1038/ncomms12917

Masmoudi, A., and P. Mandel. 1987. ADP-ribosyl transferase and NAD glycohydrolase activities in rat liver mitochondria. *Biochemistry*. 26: 1965–1969. https://doi.org/10.1021/bi00381a027

Masmoudi, A., and P. Mandel. 1989. ADP-Ribosylation in Mitochondria: Enzymatic and Non Enzymatic Reactions. *In* ADP-Ribose Transfer Reactions. Springer, New York. pp. 85–88.

Masmoudi, A., F. Islam, and P. Mandel. 1988. ADP-ribosylation of highly purified rat brain mitochondria. *J. Neurochem.* 51:188–193. https://doi.org/10.1111/j.1471-4159.1988.tb04854.x

McDonald, L.J., and J. Moss. 1994. Enzymatic and nonenzymatic ADP-ribosylation of cysteine. *Mol. Cell. Biochem.* 138:221–226. https://doi.org/10.1007/BF00928465

Menear, K.A., C. Adcock, R. Boulter, X.L. Cockcroft, L. Copsey, A. Cranston, K.J. Dillon, J. Drzewiecki, S. Garman, S. Gomez, et al. 2008. 4-[3-(4-cyclopropanecarbonylpiperazine-1-carbonyl)-4-fluorobenzyl]-2H-phthalazin-1-one: a novel bioavailable inhibitor of poly(ADP-ribose) polymerase-1. *J. Med. Chem.* 51:6581–6591. https://doi.org/10.1021/jm8001263

Messner, S., and M.O. Hottiger. 2011. Histone ADP-ribosylation in DNA repair, replication and transcription. *Trends Cell Biol.* 21:534–542. https://doi.org/10.1016/j.tcb.2011.06.001

Módis, K., D. Gerö, K. Erdélyi, P. Szoleczky, D. DeWitt, and C. Szabo. 2012. Cellular bioenergetics is regulated by PARP1 under resting conditions and during oxidative stress. *Biochem. Pharmacol.* 83:633–643. https://doi.org/10.1016/j.bcp.2011.12.014

Niere, M., S. Kernstock, F. Koch-Nolte, and M. Ziegler. 2008. Functional localization of two poly(ADP-ribose)-degrading enzymes to the mitochondrial matrix. *Mol. Cell. Biol.* 28:814–824. https://doi.org/10.1128/MCB.01766-07

Nowak, K., F. Rosenthal, T. Karlberg, M. Bütepage, A.G. Thorsell, B. Dreier, J. Grossmann, J. Sobek, R. Imhof, B. Lüscher, et al. 2020. Engineering Af1521 improves ADP-ribose binding and identification of ADP-ribosylated proteins. *Nat. Commun.* 11:5199. https://doi.org/10.1038/s41467-020-18981-w

Otto, H., P.A. Reche, F. Bazan, K. Dittmar, F. Haag, and F. Koch-Nolte. 2005. In silico characterization of the family of PARP-like poly(ADP-ribosyl) transferases (pARTs). *BMC Genomics.* 6:139. https://doi.org/10.1186/1471-2164-6-139

Palazzo, L., O. Leidecker, E. Prokhorova, H. Dauben, I. Matic, and I. Ahel. 2018. Serine is the major residue for ADP-ribosylation upon DNA damage. *eLife.* 7:e34334. https://doi.org/10.7554/eLife.34334

Pankotai, E., Z. Lacza, M. Murányi, and C. Szabó. 2009. Intra-mitochondrial poly(ADP-ribosyl)ation: potential role for alpha-ketoglutarate dehydrogenase. *Mitochondrion.* 9:159–164. https://doi.org/10.1016/j.mito.2009.01.013

Prakash, A., and S. Doublié. 2015. Base Excision Repair in the Mitochondria. *J. Cell. Biochem.* 116:1490–1499. https://doi.org/10.1002/jcb.25103

Racz, I., K. Tory, F. Gallyas Jr., Z. Berente, E. Osz, L. Jaszlits, S. Bernath, B. Sumegi, G. Rabloczky, and P. Literati-Nagy. 2002. BGP-15 - a novel poly(ADP-ribose) polymerase inhibitor - protects against nephrotoxicity of cisplatin without compromising its antitumor activity. *Biochem. Pharmacol.* 63:1099–1111. https://doi.org/10.1016/S0006-2952(01)00935-2

Ray Chaudhuri, A., and A. Nussenzweig. 2017. The multifaceted roles of PARP1 in DNA repair and chromatin remodelling. *Nat. Rev. Mol. Cell Biol.* 18:610–621. https://doi.org/10.1038/nrm.2017.53

Richter, C., K.H. Winterhalter, S. Baumhüter, H.R. Lötscher, and B. Moser. 1983. ADP-ribosylation in inner membrane of rat liver mitochondria. *Proc. Natl. Acad. Sci. USA.* 80:3188–3192. https://doi.org/10.1073/pnas.80.11.3188

Rossi, M.N., M. Carbone, C. Mostocotto, C. Mancone, M. Tripodi, R. Maione, and P. Amati. 2009. Mitochondrial localization of PARP-1 requires interaction with mitofilin and is involved in the maintenance of mitochondrial DNA integrity. *J. Biol. Chem.* 284:31616–31624. https://doi.org/10.1074/jbc.M109.025882

Slade, D. 2020. PARP and PARG inhibitors in cancer treatment. *Genes Dev.* 34: 360–394. https://doi.org/10.1101/gad.334516.119

Sumegi, K., K. Fekete, C. Antus, B. Debreceni, E. Hocsak, F. Gallyas Jr., B. Sumegi, and A. Szabo. 2017. BGP-15 protects against oxidative stress- or lipopolysaccharide-induced mitochondrial destabilization and reduces mitochondrial production of reactive oxygen species. *PLoS One.* 12: e0169372. https://doi.org/10.1371/journal.pone.0169372

Szántó, M., and P. Bai. 2020. The role of ADP-ribose metabolism in metabolic regulation, adipose tissue differentiation, and metabolism. *Genes Dev.* 34:321–340. https://doi.org/10.1101/gad.334284.119

Szczesny, B., A. Brunyanszki, G. Olah, S. Mitra, and C. Szabo. 2014. Opposing roles of mitochondrial and nuclear PARP1 in the regulation of mitochondrial and nuclear DNA integrity: implications for the regulation of mitochondrial function. *Nucleic Acids Res.* 42:13161–13173. https://doi.org/10.1093/nar/gku1089

Van Houten, B., S.E. Hunter, and J.N. Meyer. 2016. Mitochondrial DNA damage induced autophagy, cell death, and disease. *Front. Biosci.* 21: 42–54. https://doi.org/10.2741/4375

Van Ness, B.G., J.B. Howard, and J.W. Bodley. 1980. ADP-ribosylation of elongation factor 2 by diphtheria toxin. NMR spectra and proposed structures of ribosyl-diphthamide and its hydrolysis products. *J. Biol. Chem.* 255:10710–10716. https://doi.org/10.1016/S0021-9258(19)70365-2

Vivelo, C.A., R. Wat, C. Agrawal, H.Y. Tee, and A.K.L. Leung. 2017. ADPriboDB: The database of ADP-ribosylated proteins. *Nucleic Acids Res.* 45(D1):D204–D209. https://doi.org/10.1093/nar/gkw706

Vyas, S., M. Chesarone-Cataldo, T. Todorova, Y.H. Huang, and P. Chang. 2013. A systematic analysis of the PARP protein family identifies new functions critical for cell physiology. *Nat. Commun.* 4:2240. https://doi.org/10.1038/ncomms3240

Vyas, S., I. Matic, L. Uchima, J. Rood, R. Zaja, R.T. Hay, I. Ahel, and P. Chang. 2014. Family-wide analysis of poly(ADP-ribose) polymerase activity. *Nat. Commun.* 5:4426. https://doi.org/10.1038/ncomms5426

Welsh, C.F., J. Moss, and M. Vaughan. 1994. ADP-ribosylation factors: a family of approximately 20-kDa guanine nucleotide-binding proteins that activate cholera toxin. *Mol. Cell. Biochem.* 138:157–166. https://doi.org/10.1007/BF00928458

Williams, E.G., Y. Wu, W. Wolski, J.Y. Kim, J. Lan, M. Hasan, C. Halter, P. Jha, D. Ryu, J. Auwerx, and R. Aebersold. 2018. Quantifying and localizing the mitochondrial proteome across five tissues in a mouse population. *Mol. Cell. Proteomics.* 17:1766–1777. https://doi.org/10.1074/mcp.RA118.000554

Yang, C.S., K. Jividen, A. Spencer, N. Dworak, L. Ni, L.T. Oostdyk, M. Chatterjee, B. Kuśmider, B. Reon, M. Parlak, et al. 2017. Ubiquitin Modification by the E3 Ligase/ADP-Ribosyltransferase Dtx3L/Parp9. *Mol. Cell.* 66:503–516.e5. https://doi.org/10.1016/j.molcel.2017.04.028

Supplemental material

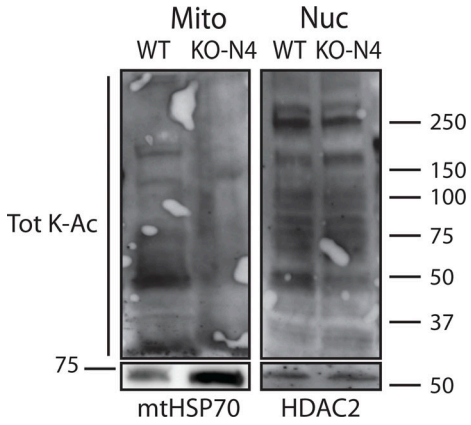

Figure S1. **Supplement to Fig. 2.** Related to Fig. 2 WB anti-acetylated lysine on mitochondrial (Mito) and nuclear (Nuc) extracts from WT and N4-KO cells. Lower panels represent control blots for mitochondrial and nuclear markers (mtHSP70 and HDAC2). Tot K-Ac, total acetylated lysine.

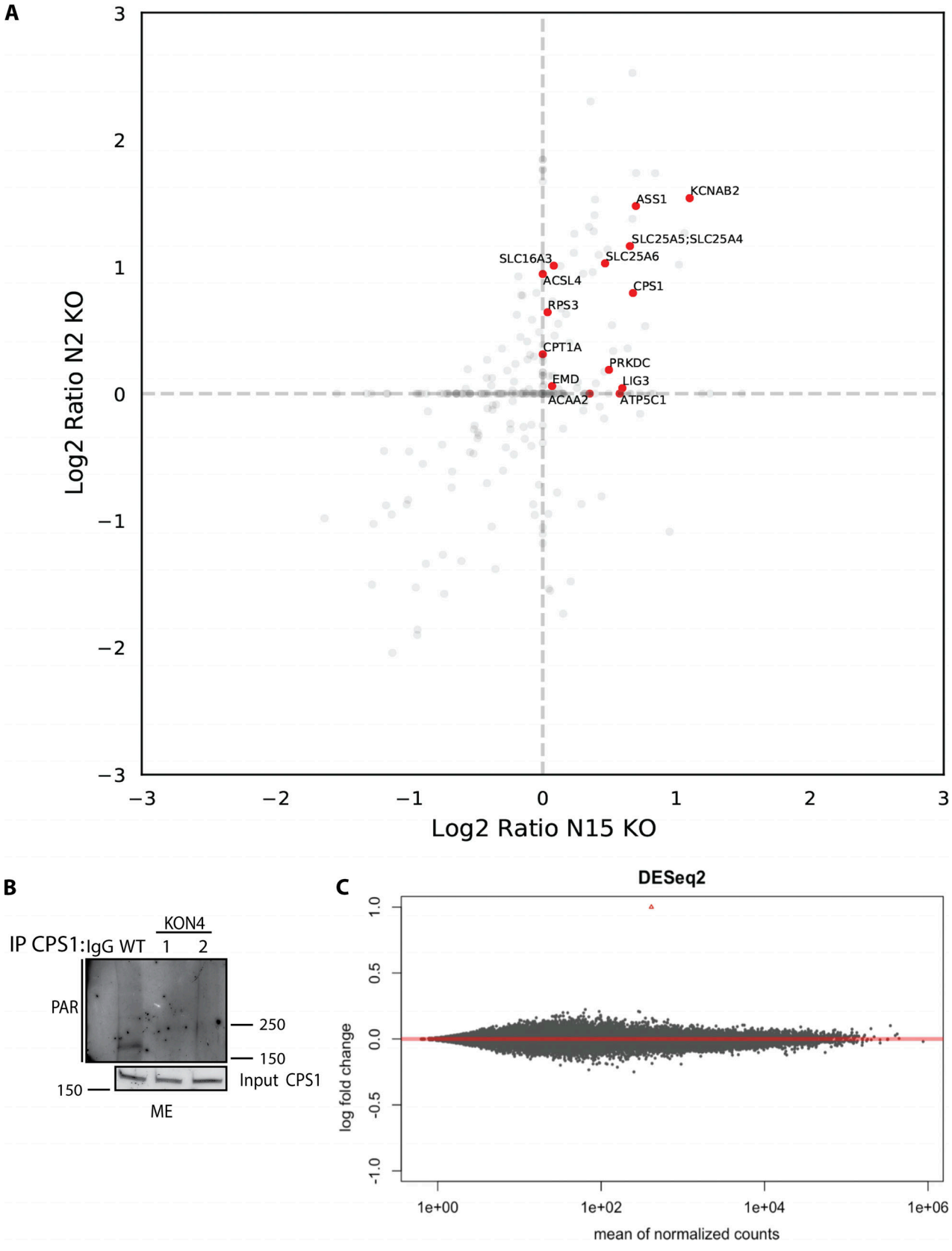

Figure S2. **Supplement to Fig. 4.** Related to Fig. 4. **(A)** SILAC-based enrichment of PARylated proteins identified in WT nonstressed HeLa cells using either NEURL4 KO1 or KO2 cells as a background. **(B)** IP assay showing suppression of CPS1 PARylation in the absence of NEURL4. **(C)** Profiling of DEGs identified in NEURL4 KO1 and KO2 cells as compared with WT parental HeLa cells by RNA-seq and differential gene expression analysis by DESeq2. DEGs, differential expressed genes; ME, mitochondria extracts.

Video 1. **Time-lapse epifluorescence microscopy showing WT mice normal sperm movement.**

Video 2. **Time-lapse epifluorescence microscopy showing increased sperm agglutination for NEURL4$^{+/-}$ heterozygous mice.**

Table S1 and Table S2 are provided online as separate Excel files. Table S1 shows raw proteomic data and a list of potential NERL4 targets. Table S2 is a differential genes list in NEURL4 WT and KO cells.